Magnetohydrodynamic and thermal analysis of PbLi flows in poloidal channels with flow channel insert for the EU-DCLL blanket

F. R. Urgorri[1], S. Smolentsev[2], I. Fernández-Berceruelo[1], D. Rapisarda[1], I. Palermo[1], A. Ibarra[1]

[1] CIEMAT-LNF, Av. Complutense 40, Madrid 28040, Spain
[2] UCLA-MAE,43-133 Engineering IV, Los Angeles, California, USA

E-mail: fernando.roca@ciemat.es

December 2017

Abstract. Magnetohydrodynamic (MHD) processes are known to be critically important for the Dual Coolant Lithium Lead (DCLL) breeding blanket (BB) concept. In order to minimize the MHD pressure drop in the European DCLL blanket design, the liquid metal breeder (PbLi) is decoupled electrically from the ferritic-martensitic structure (EUROFER) using insulating ceramic-based flow channel inserts (FCIs). The impact of the FCI on the velocity profile and the pressure drop in the DCLL front poloidal channels is studied. Two-dimensional momentum and induction equations for fully developed flows are solved numerically using the ANSYS-Fluent simulation platform under DCLL-relevant conditions (Ha=$7.57 \cdot 10^3$, Re=$2.27 \cdot 10^4$). Velocity and pressure drop in the PbLi flows have been computed first for a channel without FCI and then for three possible alumina-based FCI design: two types of sandwich FCI and one naked FCI. In order to analyze thermal effects in the blanket, the obtained velocity profiles are used as inputs to solve the 3D energy equation. The computations of the temperature distribution in the DCLL poloidal front channel with a prototypical exponentially varying heat generation profile are obtained using convective boundary conditions. Results show the effect of the FCI and MHD phenomena on heat transfer.

Keywords: MHD, DCLL, FCI, Alumina, DEMO
Submitted to: *Nucl. Fusion*

1. Introduction

The breeding blanket (BB) is a crucial system for future D-T fusion power plants. It is a system designed, among other functions, to ensure the needed tritium self-sufficiency of the plant. Besides the elements needed to accomplish this objective, any viable BB must include mechanisms that perform other important functions. Indeed, the BB has to be able of extracting the thermal power from the reactor for the subsequent energy conversion while providing the required neutron shielding to the vacuum vessel and the toroidal field coils.

In the framework of the EUROfusion Consortium Program there are four BB concepts under consideration, which are: Helium Cooled Pebble Bed (HCPB), Helium Cooled Lithium Lead (HCLL), Water Cooled Lithium Lead (WCLL), and Dual Coolant Lithium Lead (DCLL) [1]. The last three concepts are based on lead-lithium (PbLi) as tritium breeder, neutron multiplier and tritium carrier. Magnetohydrodynamics (MHD) effects arise in the PbLi channels of these blankets as they are immersed into a very intense magnetic field. Being the PbLi an excellent electrical conductor, MHD effects will be very relevant for the PbLi dynamics. As the MHD phenomena can produce important pressure drops in the PbLi flows and significantly impact the blanket functionality, MHD analyses are of primary interest from the design perspective.

In the PbLi flows, the main dimensionless numbers that describe the regime of the system are the Reynolds number: $Re = \rho U_0 D/\eta$, the Hartmann number: $Ha = B_0 a\sqrt{\sigma/\eta}$ and the Grashof number: $Gr = g\beta\Delta T\rho^2 b^3/\eta^2$. Here, U_0 is the mean velocity of PbLi, B_0 is the external magnetic field, a is the half of the channel length along the magnetic field direction, b is the half of the channel length along the direction of the heat flux, D is the hydraulic diameter of the channel, ρ is the PbLi density, ΔT is the characteristic temperature difference, g is the gravitational acceleration, β is the volumetric thermal expansion coefficient, η the PbLi dynamic viscosity and σ is the PbLi electrical conductivity. The Grashof number represents the ratio between the buoyancy forces and the viscous forces while the square of the Hartmann number represents the ratio between the Lorentz forces and the viscous forces. In the European PbLi-based blanket concepts, the order of magnitude of the Hartmann number varies from 10^3 to 10^4. These high values imply a dominant role of the MHD interactions over viscous effects in the PbLi dynamics.

MHD pressure losses are directly related with the electrical coupling between the liquid metal and the metallic structure. In order to mitigate the MHD pressure drop, ceramic structures called flow channel inserts (FCIs) have been proposed [2]. This work is based in the EU-DCLL design which includes FCIs embedded in the PbLi channels [3]. These FCIs are based on alumina, a material with excellent insulating properties. The design of the FCI is not concluded, as several aspects need to be studied from the theoretical, experimental and manufacturing point of view [4]. Three different alumina-based FCI design options are under consideration for the EU-DCLL: a thin sandwich design (0.5 mm steel-0.1 mm alumina-0.5 mm steel) [5] which is considered the baseline option, a thick sandwich design (1 mm steel-5 mm alumina-1 mm steel) and a naked alumina design of 5 mm thick [4].

MHD pressure drops and velocity profiles of a DCLL central front channel have been computed for the 3 FCI designs. 2D fully developed flow models have been employed for this purpose following the methodology firstly used for the US-DCLL blanket with SiC_f/SiC FCI [6]. 3D heat transfer analyses have been carried out too using the MHD velocity profiles as inputs.

2. Description of the EU-DCLL blanket

As other PbLi-based BB, the EU-DCLL is based on eutectic PbLi as neutron multiplier and tritium breeder. However, in this blanket concept the PbLi acts also as the primary coolant (self-coolant). For this reason the liquid metal flows at much higher velocities ($\sim$ 1 cm/s) than in other PbLi based breeding blanket concepts. The blanket design also includes helium (He) for cooling the structure, especially the first wall (FW) which supports the highest thermal loads. The structural material is the reduced activation ferritic-martensitic steel (EUROFER). Since the design of the EU-DCLL is evolving, the assessments here presented are based on the most recent available design [7].

The blanket is divided into 18 equal sectors along the toroidal direction. Each of these sectors consists of 5 segments; 3 of them located in the outboard zone (OB) while the other 2 are located in the inboard zone (IB). Unlike other DCLL designs (e.g. [8]), the segments of the EU-DCLL are formed by modules (8 modules each). Figure 1 shows the multi-module configuration of one sector. The IB equatorial modules are immersed in a very intense magnetic field ($B_0 \sim 9$ T) while the OB modules are subjected to a lower, but still high magnetic field ($B_0 \sim 4$ T).

The modules have slightly different sizes and shapes depending on their poloidal location. They are attached to a common back supporting structure (BSS). The BSS has not only a mechanical function but it also acts as manifold for the PbLi and He flows. For this reason, two big PbLi rectangular channels and four He channels are placed in the BSS along

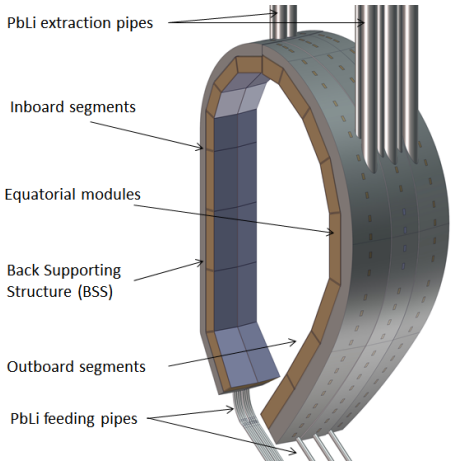

Figure 1. Geometrical configuration of one DCLL sector showing 3 OB segments and 2 IB segments, each one composed of a series of modules and a BSS.

the poloidal direction (see figure 2). These channels feed the modules with cold PbLi/He and collect both coolants once they have been heated.

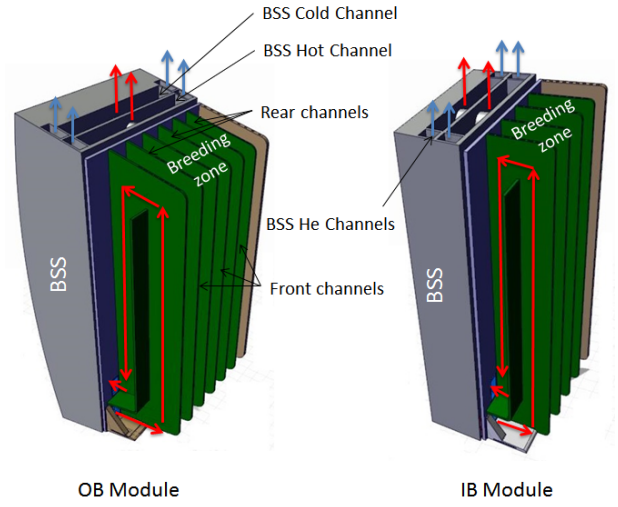

Figure 2. (left) OB equatorial module; (right) IB equatorial module. The PbLi flows are shown in red and the He flows are shown in blue.

The design activities of the DCLL focus on the equatorial modules as they support one the highest thermal and neutronic loads. The PbLi enters the module at 300°C through the so called cold channel of the BSS and it exists the module at 550°C through the hot channel of the BSS. In figure 2, the geometry of the equatorial modules is shown as well as a sketch of the PbLi flow path.

The front part of the modules, where the majority of the tritium is generated, is called the breeder zone. The breeder zone is formed by two kind of poloidal channels: the front channels and the rear channels. The front channels are located next to the FW and supports a higher thermal flux than the rear channels which are placed further from the plasma.

Among other criteria, the DCLL modules have been designed minimizing the complexity of the PbLi flow path. Indeed, most of the PbLi flow path consists of straight parallel poloidal channels. The magnetic field points to the toroidal direction. Thus, it lays transversely to the PbLi flow. The straight rectangular section channels will contribute to the total MHD pressure drop due to the forces created by the induced electrical currents. In order to mitigate this contribution, FCIs are placed embedded in the PbLi channels. The flow is consequently divided into two regions called bulk flow and gap flow following the terminology first employed in [6]. If the insulation is not perfect, both regions can interact electrically through the FCI. Inside the bulk flow, the induced currents will point into the radial direction (perpendicular to the velocity and magnetic fields) in most of the cross sectional plane (core flow). Next to the walls the currents behave differently depending on the interaction with the FCI and the structural walls forming boundary layers. The boundary layers perpendicular to the external magnetic field are usually called Hartmann layers while the boundary layers parallel to the magnetic field are usually called side layers. The channel walls next to the boundary layers are usually referred as Hartmann walls and side walls, respectively. Figure 3 shows a sketch of the cross section of one DCLL front central channel.

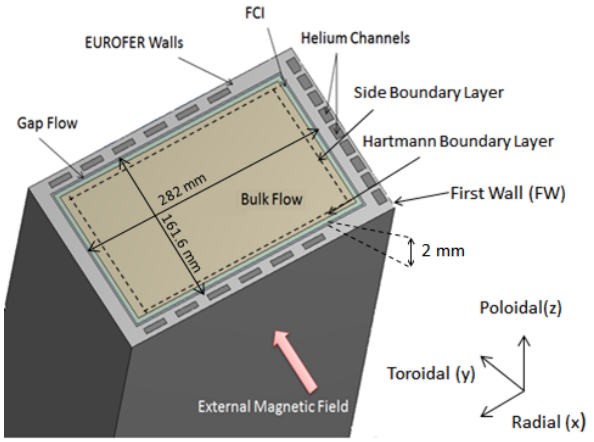

Figure 3. Sketch of the cross section of one DCLL central front channel showing the bulk flow, the gap flow, the FCI, the He channels and the MHD boundary layers.

The FCI is a crucial component for the DCLL blanket. Several activities are being carried out for testing the properties and manufacturing feasibility of the different FCI designs under consideration [4, 5, 9]. The result from these activities and the MHD simulations and experiments will be used for the final FCI design selection. Figure 4 shows a sketch of the

three FCI designs under consideration for the EU-DCLL with their respective dimensions.

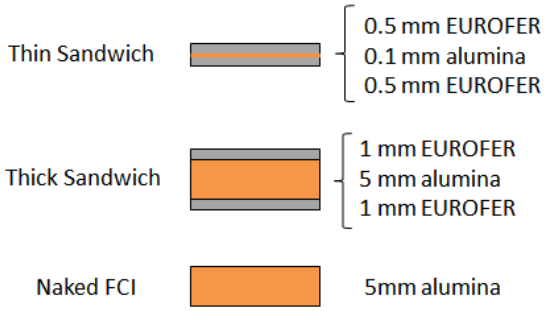

Figure 4. FCI design options under consideration for the EU-DCLL showing the alumina in orange and the EUROFER in grey.

The characteristic dimensionless numbers of the EU-DCLL channels are exposed in table 1 and table 2. In order to estimate the Grashof number in the different channels, the characteristic temperature difference ΔT have been estimated considering a simplified 1D conduction model. In other words, $\Delta T = \overline{q} \cdot b^2/\kappa$, where $\overline{q}$ is the average volumetric heating in the channel, b is the half of the channel length along the heat flux direction and κ is the thermal conductivity of PbLi. The Grashof number computed with this method is most likely an overestimation of the real value but it provides a preliminary value until more detailed calculations are performed (section 6).

Table 1. Characteristic dimensionless constants of the DCLL outboard channels.

	Outboard segment			
	Breeding zone channels		BSS channels	
	Front	Rear	Hot	Cold
Ha	$7.63 \cdot 10^3$	$8.46 \cdot 10^3$	$5.79 \cdot 10^4$	$4.18 \cdot 10^4$
Re	$2.72 \cdot 10^4$	$3.63 \cdot 10^4$	$3.65 \cdot 10^5$	$1.39 \cdot 10^5$
Gr	$5.98 \cdot 10^{11}$	$1.47 \cdot 10^{11}$	$5.19 \cdot 10^8$	$3.48 \cdot 10^7$

Table 2. Characteristic dimensionless constants of the DCLL inboard channels.

	Inboard segment			
	Breeding zone channels		BSS channels	
	Front	Rear	Hot	Cold
Ha	$1.75 \cdot 10^4$	$1.91 \cdot 10^4$	$9.19 \cdot 10^4$	$6.84 \cdot 10^4$
Re	$2.94 \cdot 10^4$	$4.40 \cdot 10^4$	$2.57 \cdot 10^5$	$1.88 \cdot 10^5$
Gr	$7.19 \cdot 10^{11}$	$3.16 \cdot 10^{10}$	$1.58 \cdot 10^8$	$1.56 \cdot 10^8$

3. Mathematical and computational model

The present analyses are applied to the central front poloidal channel of the breeding zone of one DCLL OB equatorial module. This model studies the straight regions of the channel and, thus, it does not take into account any effect produced by the 3D elements of the geometry. Its main objective is to analyze and compare the response of different alumina based FCI designs (figure 4).

The model employed for the flow computation is 2-dimensional. The applicability of 2D MHD models in straight channels with FCI under transverse magnetic fields is discussed in [6]. Far from the 3D elements of the design (inlets, bends...) and when neither transient effects nor buoyancy effects are considered, the flow is expected to be fully developed. Under these conditions, there are no axial currents (all of them are cross sectional) and there is no dependence with the axial coordinate (z).

Starting from the MHD equations written in B-formulation (based on $\vec{u}$ and $\vec{B}$ as variables), the general set of 6 MHD equations (vectorial momentum and induction equations) with 6 variables can be reduced to a set of only two equations: a 2D momentum (1) and a 2D induction equation (2). These equations are written in terms of only two variables: the axial velocity $U(x,y)$ and the induced magnetic field $B_i(x,y)$ which lays along the axial direction too (cross sectional currents).

$$\eta\left(\partial_{xx}U + \partial_{yy}U\right) - \partial_z p + \frac{B_0}{\mu}\partial_y B_i = 0 \quad (1)$$

$$\mu^{-1}\left(\partial_x\left(\sigma^{-1}\partial_x B_i\right) + \partial_y\left(\sigma^{-1}\partial_y B_i\right)\right) + B_0\partial_y U = 0 \quad (2)$$

In (1) and (2), B_0 is the external toroidal (y) magnetic field and η, σ and μ are the dynamic viscosity, the electrical conductivity and the magnetic permeability of the materials of the system (PbLi, EUROFER and alumina). The pressure gradient is considered constant. Thus, the variation of the pressure (p) along the axial (poloidal) direction is linear.

In order to obtain convergence it is necessary to adapt the computational mesh to the heavy MHD requirements. So as to have enough resolution to resolve the Hartmann layers, it is necessary to provide a sufficient amount of mesh points in the layer, whose thickness scales with Ha^{-1}. Following the criteria described in [10] hyperbolic mesh gradients have been applied from the center of the flow to the layers. Figure 5 shows a part of the computational mesh used for the thin sandwich FCI computation. The meshes used for the other two FCI designs have the same kind of gradients.

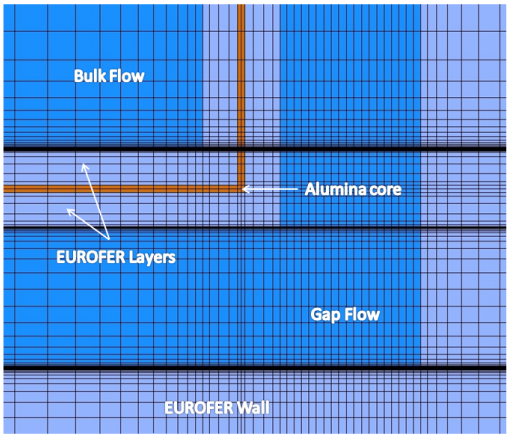

Figure 5. Detailed part of the computational mesh used for the thin sandwich FCI concept.

The MHD velocity profiles computed with the 2D model have been used as an input for a stationary 3D heat transfer analysis. The energy equation (3) has been solved for the three FCI designs:

$$\rho C_p U \partial_z T - \partial_i \left(\kappa \partial^i T\right) = S_h \quad (3)$$

$$S_h = q \exp\left(-mx\right) \quad (4)$$

Where C_p is the specific heat of the materials and κ their thermal conductivities. The source S_h (4) represents the heat generated by the interacting neutrons and photons. A prototypical exponential shaped function along the radial direction (x) has been used. The parameters q and m have been taken according to the result of the best fitting of the neutronic data concerning the EU-DCLL [11]. In the case of the OB equatorial module front channels the parameters are: $q = 7.41$ W/cm^3 and $m = 6.3$ m^{-1} (the point x = 0 is defined at the external side of the FW).

Table 3. Main input parameters.

Input Parameter	Value
Toroidal Size; 2a (mm)	161.6
Radial Size; 2b (mm)	282
Length; L (m)	2
Gap Thickness; t_{gap} (mm)	2
First Wall thickness; t_{fw} (mm)	18.64
Radial Walls thickness; t_{sw} (mm)	13.48
Rear Wall thickness; t_{rw} (mm)	16.5
Flow rate; F_0 (L/s)	0.775
PbLi inlet temperature; T_{in} (°C)	308
First wall He inlet temperature; $T_{He\ FWin}$ (°C)	318
First wall He outlet temperature; $T_{He\ FWout}$ (°C)	433
Radial walls He average temperature; $T_{He\ SW}$ (°C)	436
External Magnetic Field; B_0 (T)	4.147

The dimensions and magnetic conditions used in the simulations are the ones of one DCLL outboard equatorial module central front channel (figure 3). The FW and the radial walls are cooled with He flowing in rectangular channels inside the steel. The He channels introduce anisotropy in the wall electric conductivity that could alter the behavior of the PbLi flow. However, according to previous studies these effects are expected to be small and located next to the MHD boundary layers [12]. As a first approach, the thicknesses of the steel walls have been readjusted to effective values extrapolated through the volume fraction steel/helium of the walls. The main input data used in the simulations are summarized in table 3.

The mechanical and thermal properties of PbLi [13] and EUROFER [14] used in the computations are exposed in table 4. The electrical conductivity of both materials [15, 16] is depicted as well. The expected PbLi inlet and outlet temperatures in the front channel are approximately 300°C and 500°C, respectively. As a consequence, an average temperature of 400°C has been used for the PbLi properties. In this channel, EUROFER temperatures are expected to be in the range of 400-550°C, reaching the maximum temperature in the FCI layers. Taking into account the small variation of the EUROFER properties in this range, these at 500°C has been used for the computations.

The electric properties of the alumina considered for the present FCIs have been measured in recent experimental campaigns [4] whose results showed a very good electrical insulating capability in a large temperature range (200-600°C). Alumina thermal properties have been taken from the commercial specifications of the KA997 aluminum oxide.

Table 4. Materials properties.

	PbLi	EUROFER	Alumina
ρ (kg/m^3)	9720	7608	3950
σ (S/m)	$7.63 \cdot 10^5$	$8.33 \cdot 10^5$	10^{-8}
η (Pa s)	$1.497 \cdot 10^{-3}$	–	–
Cp (J/kg K)	189	730	880
κ (W/m K)	15.14	30.35	28

4. Validation case

The system of equations (1) and (2) has been solved using the MHD capabilities of the ANSYS-Fluent platform. Previous works have tested the capabilities of this platform against experimental data [17].

However, Fluent computations of fully developed flows using B-formulation need to be validated, specially for high Hartmann numbers. For this purpose, two flows with known analytic solutions have been computed with Fluent: the Shercliff flow [18] and the Hunt flow [19]. The first system consist of

a rectangular section channel with perfectly insulating walls under a transverse magnetic field. The second system is almost equal to the first one but the Hartmann walls (perpendicular to the magnetic field) have an arbitrary wall conductance ratio (C_w). The side walls (parallel to the magnetic field) are still perfectly insulating.

For plotting the analytic solution, the reformulation of the original hyperbolic expressions in terms of exponential functions used in [20] has been employed. The channel dimensions and the magnetic field used as inputs for these computations are the same than the ones that are used for the rest of the MHD calculations (table 3). Therefore, the Hartmann number is $7.63{\cdot}10^3$. The wall conductance ratio used for the Hunt case is $C_w = 0.05$.

Figure 6 shows the velocity profile obtained with Fluent along a line perpendicular to the magnetic field that goes through the center of the channel (y=0). Results are depicted next to the side boundary layers normalized with respect to the core velocity. The computational solutions are compared with the analytic solutions along the same curve. Results show a good match between computational results and analytic solutions.

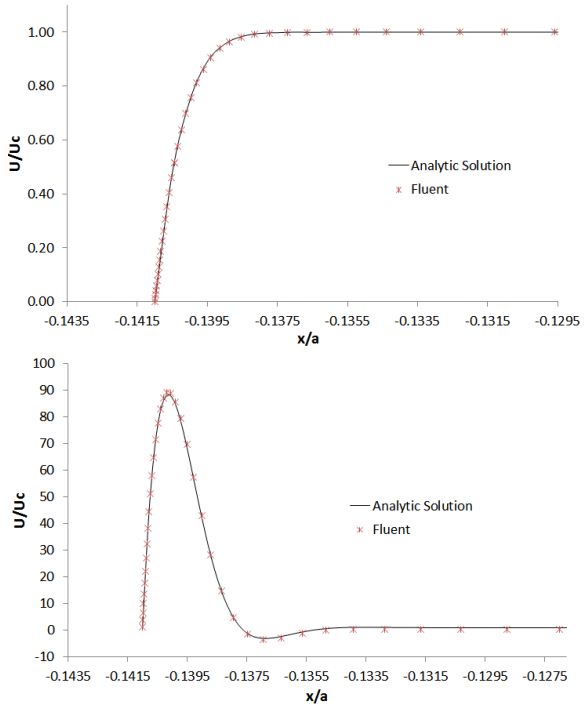

Figure 6. Comparison between Fluent result and analytic solution [20]. (up) Shercliff flow; (down) Hunt Flow.

5. MHD fully developed flow results

Results for 3 different FCIs concepts have been obtained. For comparison purposes the velocity profile of the central front channel without FCI has been calculated as well. The obtained velocity profiles are exposed in figure 8.

Analyzing the velocity profiles it can be deduced that the alumina is able to effectively decouple the bulk flow from the gap flow. Indeed, the naked alumina FCI case exhibits in the bulk flow the characteristic flat profile of a rectangular channel with perfectly insulating walls [18]. This implies that there is no interaction between the bulk flow and the gap flow. For the two sandwich-like FCIs designs there is also an effective decoupling between the bulk flow and the gap flow, but in these cases EUROFER layers are in contact with the PbLi. Those layers act as thin conducting walls which produce the characteristic MHD flow of a channel with conducting walls: a flat core and two jets in the side layers [21].

Qualitatively, the gap flow behaves similarly for the three FCI designs. Figure 7 shows the current distribution of the thin sandwich FCI case. It can be observed that the currents in the gaps next to the side boundary layers (side gaps) flow mainly in the toroidal direction, parallel to the external magnetic field. As a consequence, the Lorentz forces in these gaps are small and viscous effects are dominant. It causes an almost parabolic profile along the radial direction (figure 9). The opposite situation takes place in the gaps next to the Hartmann boundary layers (Hartmann gaps). In these regions the currents are mainly perpendicular to the external field and the Lorentz forces are intense. Therefore, the flow is almost static and the vast majority of the gap flow runs through the side gap.

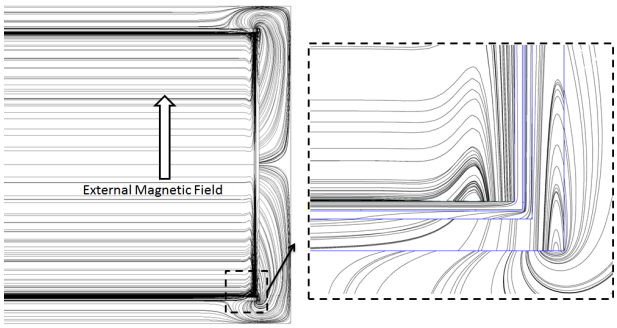

Figure 7. Current distribution for the DCLL central poloidal channel with a thin sandwich FCI.

The total flow rate in the four cases is the same (0.775 L/s) but the MHD phenomena affect the flow partitioning between the bulk and the gap regions. For the sandwich like FCI designs, the high resistance that

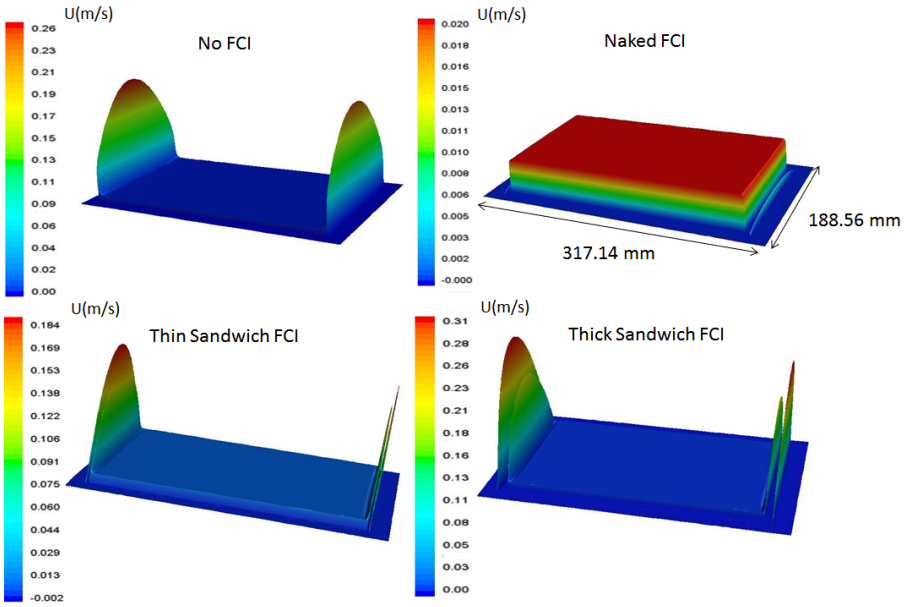

Figure 8. Velocity profiles for the central front channel with 3 different FCI designs and without FCI.

the MHD forces impose to the bulk flow makes that a significant amount of flow rate goes through the side gaps where the resistance is much lower causing high velocity jets in the gap flow. Besides the MHD effects, the geometry of the channels has an impact on the velocity scale as the cross sectional area depends on the FCI thickness. As a consequence, mean velocities are different even the flow rate is not. In order to compare the profiles, a 2D plot along a straight radial line that crosses the center of the channel is presented in figure 9.

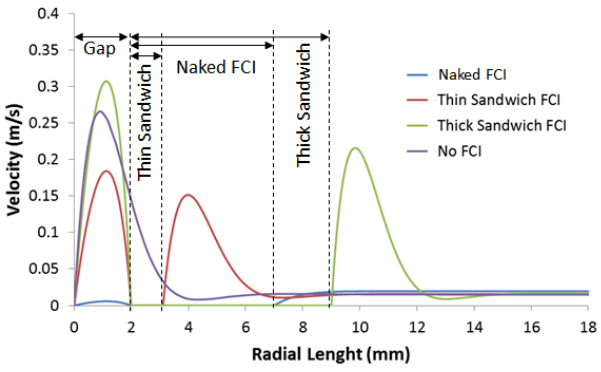

Figure 9. Axial velocity next to the side wall along a radial line that crosses the center of the channel(y = 0).

From these 2D fully developed analyses useful information can be obtained. The pressure drop per unit length associated to the different FCI designs is exposed in table 5. The pressure drop reduction factor associated to each FCI design is shown as well. This magnitude is defined as the ratio between the pressure drop of a channel without FCI $(\Delta p/\Delta z)_0$ and the pressure drop of the same channel with FCI.

Table 5. Pressure drop associated to the three FCI designs.

	$\frac{\Delta p}{\Delta z}\left(\frac{Pa}{m}\right)$	$\frac{\left(\frac{\Delta p}{\Delta z}\right)_0}{\left(\frac{\Delta p}{\Delta z}\right)}$
No FCI	34224.6	–
Naked FCI	36.1	948.05
Thin Sandwich FCI	1739.5	19.67
Thick Sandwich FCI	3861.1	8.86

The naked FCI provides the best pressure drop mitigation as it has no EUROFER in contact with the bulk flow which reduces significantly the density of induced currents. In the sandwich like FCI designs the thickness of the EUROFER layer is the parameter that determines the pressure drop mitigation. No matter how perfect the electrical insulation properties of the alumina core are, the steel layer reduces significantly the FCI effectiveness.

In table 6, the velocity of the flat core in the bulk flow is shown together with the average velocity. The peak velocity of the jets at both sides of the FCI next to the side wall is shown as well. Moreover, the percentage of flow that goes through the bulk and the gap is exposed in table 7. The total flow rate (F_0) is the same in every case (0.775 L/s).

From the computational results it can be observed that for all FCI design there is a very small percentage of flow that goes through the Hartmann gap. This situation is especially pronounced for the naked FCI design. In the sandwich-like designs, a high flow rate

Table 6. Characteristic velocities of the fully developed flow.

	U_{core} (cm/s)	U_{avg} (cm/s)	U_{jets} (cm/s)	
			Bulk	Gap
No FCI	1.48	1.17	26.60	–
Naked FCI	1.97	1.88	–	0.59
Thin Sandwich FCI	1.59	1.74	15.41	18.72
Thick Sandwich FCI	1.64	1.95	21.51	30.69

Table 7. Flow distribution.

	$\frac{F_{Bulk}}{F_0}$(%)	$\frac{F_{Gap}}{F_0}$(%)	
		Side	Hartmann
No FCI	100	–	–
Naked FCI	99.77	0.2297	0.0003
Thin Sandwich FCI	92.87	7.113	0.017
Thick Sandwich FCI	88.15	11.809	0.041

goes through the side gaps which is translated into high velocities jets in these regions. This effect is more prominent for the thick FCI design.

The results obtained in the present work are qualitatively in good agreement with previous studies performed with 2D fully developed models for the US-DCLL [6]. Quantitatively, results are different because conditions such as geometrical dimensions of the channel, the external magnetic field and the FCI design are also different.

6. Heat transfer analyses

Heat transfer analyses have been performed for the central front channel using the calculated MHD velocity profiles as fixed inputs for solving (3). For simplicity, instead of computing the complete He flow inside the EUROFER, convective boundary conditions have been considered at the external side of the walls.

$$q = h_{He}(T_{wall} - T_{He}) \tag{5}$$

The convective boundary condition requires providing the helium temperature (T_{He}) and the heat transfer coefficient (h_{He}) in each wall of the channel. Instead of using an average He temperature, the results of a 1D heat transfer code developed for the DCLL design activities (PLATOON code [7]) have been employed. This code models the complete OB equatorial module. It discretizes the PbLi and He flows only along their respective flow directions. Both flows are connected across solid materials with the appropriate surfaces, thicknesses and thermal properties. Heat generation inside the components of the model is also considered when needed. This 1D code does not take into account the specific shape of the PbLi and He velocity profile. Instead, it considers heat transfer between the fluids and the solid walls occurs by convection (5) and calculates h by means of empirical correlations of the Nusselt number. For the PbLi, the heat transfer coefficient is based on an experimental correlation obtained for flows under transverse fields and insulating walls [22]. At the interface between the steel and the He the code uses the Gnielinski correlation [23].

According to the results of the 1D model, the He temperature in the FW channel follows an almost linear profile. The He enters the bottom part of the channels at 318°C and leaves the top part at 433°C. This same linear profile has been imposed as boundary condition in the FW He channels for the present heat transfer calculations. An average heat transfer coefficient of 3084 W/m^{2}K has been established in the FW He channels based on the 1D model outputs.

Once the He exits the FW channels it descends through the radial walls. The 1D model predicts an increment of only 4°C in the helium temperature between the top part and the bottom part of the radial walls (from 434°C to 438°C). Taking into account this almost uniform temperature, a constant He temperature of 436°C has been considered in both radial walls for the present heat transfer computations. Like in the FW He channels, an average heat transfer coefficient has been established in the radial walls He channels (3366.5 W/m^{2}K). The He and PbLi boundary temperature values are also exposed in table 3.

The design of the DCLL module does not include He channels in the rear wall. A zero flux boundary condition has been imposed as a first approximation.

Results of temperature contours for the central radial-poloidal plane and for the mid sectional plane are exposed in figure 10 and figure 11, respectively.

Analyzing figure 10 and figure 11 it can be observed the effect of the MHD velocity profile over the heat transfer. On the one hand, the exponential generation profile produces important temperature differences along the radial direction. On the other hand, the small velocities in the Hartmann gaps turn them into hot regions. The result of both phenomena are the oval shape of the temperature contours that can be observed in figure 11.

From this analysis the heat losses from the PbLi to the He circuit can be derived. It is worth mentioning that the heat flows through the channel walls in both directions. Locally, there are regions where the PbLi is colder than the He. In this regions, the heat flows from the He to the PbLi. This is true mainly next to the inlet. However, in the majority of the system the PbLi is hotter than the He which is translated into a heat flux from the PbLi to the He. By integrating the heat flux along the contact surface the total heat that

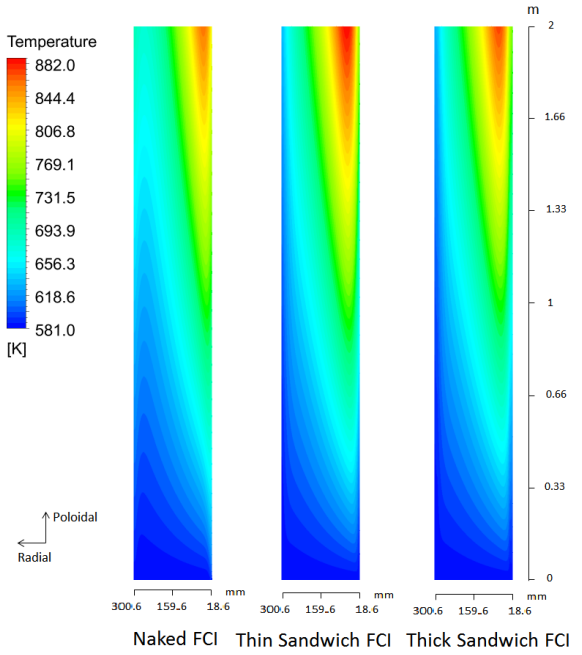

Figure 10. Temperature contours in the central radial-poloidal plane.

goes from the PbLi to the He can be obtained (table 8). The total amount of heat generated in the system is q_0 = 0.2807 MW which can be obtained by integrating (4) in the channel volume.

Table 8. Net heat fluxes through the channel walls (from PbLi to He).

	q_{FW} (W)	q_{Radial} (W)	$\frac{q_{He}}{q_0}$ (%)
Naked FCI	21926.83	10890.78	11.69
Thin Sandwich FCI	10890.26	810.88	4.17
Thick Sandwich FCI	10675.39	9185.24	7.07

The naked FCI design develops small velocities in the gap next to the FW compared with the other two designs. For this reason the heat flux from the PbLi to the He circuit in the FW is much higher. In figure 10 and figure 11 it can be observed that the temperature next to the FW is lower for the sandwich-like designs as the side jets cool the FW more efficiently.

The almost stagnant flow in the Hartmann gap made that, in these regions, the heat flows almost exclusively by conduction along the sectional planes. This causes that the heat flux through the radial walls is significantly affected by the thickness of the FCI. The heat generated in the bulk zone is mostly removed by the PbLi flow while the heat generated in the Hartmann gap and in the FCI is removed either by the cooling effect of the bulk flow or the He flow, depending on the zone. In the case of the thin FCI there is more heat generated in the bulk zone because of its smaller

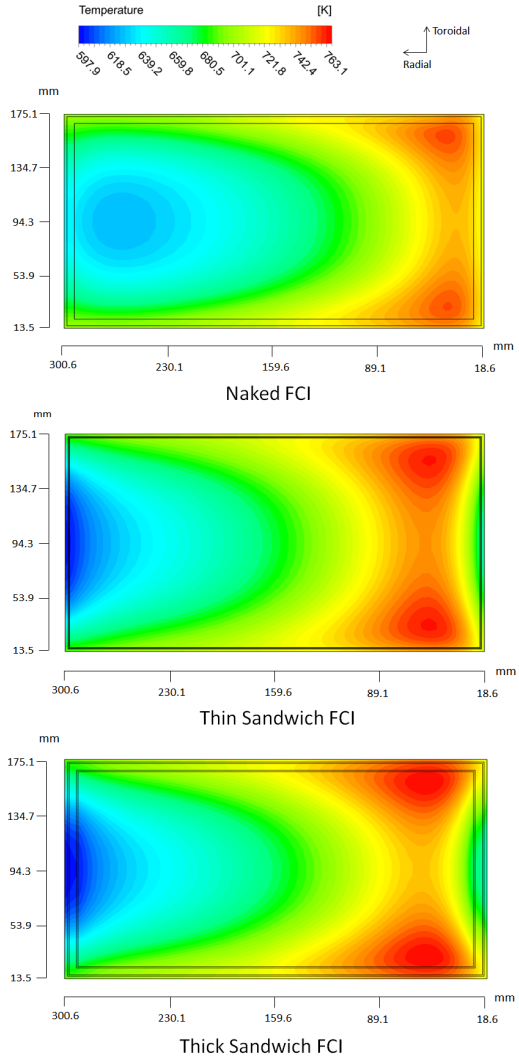

Figure 11. Temperature contours in the middle section (z=L/2).

volume while in the other 2 designs there is more heat produced inside the FCI. For this reason, in the thick designs the magnitude of the heat transferred to the Hartmann gap and extracted by the helium flow is higher than in the case of the thin FCI (table 8).

According to the present calculations, the Grashof number in the OB front channels is Gr = $2.93 \cdot 10^{10}$ which is one order of magnitude less than the preliminary estimations given in table 1. This value is more accurate but still not completely representative as the buoyancy forces have not been taken into account in the pressent calculations. Regardless, considering the high Grashof number obtained, it is expected that the temperature variations in the channel cross section (figure 11) will generate buoyancy effects that can affect the velocity profile [24] and consequently the heat transfer. In order to analyze the buoyancy phe-

nomenon, magneto-convective computations including the coupling between temperature field, the magnetic field and the velocity field are planned to be carried out in future works.

7. Discussion

Sandwich-like FCI and naked FCI present different benefits and drawbacks. Velocity profiles of the sandwich-like designs are significantly different compared with the naked design. The EUROFER layers of the sandwich FCI allow tangent currents to penetrate in it. This entails to the jet formation next to the side boundary layers. Besides, the pressure drop reduction factor of the sandwich-like concepts is severely affected by the thickness of the EUROFER layers. From this point of view, the thick sandwich design is the less effective option of the ones studied.

Not having any steel layers, the naked FCI provides the best pressure drop mitigation. However, the flow partitioning between the bulk flow and the gap flow is very unalike for this design. The small flow rate through the gap causes hotter regions next to the FW in comparison with the sandwich-like designs. For the naked FCI more than 11% of the energy generated in the channel goes to the He circuit. From this point of view, the thin sandwich FCI design provides the best thermal behavior as only 4.17% of the energy generated in the channel goes to the He circuit.

The viability of any FCI design depends on more factors than the ones analyzed, which are planned to be studied in future. For example, the jets of the sandwich-like concepts provide a better cooling of the FW but the high velocities that exhibit (0.1 m/s) could be unacceptable from the corrosion point of view [25, 26]. Besides, the temperature gradients between the faces of the FCIs might lead to important thermal stresses. This could be critical for the sandwich like concepts where different thermal expansion coefficients of the alumina and the EUROFER would produce unacceptable stresses in the FCI [4]. These deformations could potentially affect the flow partitioning and the gap flow velocity profile as well. The pressure difference between the gap flow and the bulk flow can also produce stresses in the FCI. Pressure equalization holes or slots (e.g. [27]) have been proposed for solving this problem. However, they present important manufacturing difficulties. Experimental analyses are planned for testing the FCI performance in PbLi loops under relevant magnetic field. They could help determining whether this pressure difference will present mechanical problems for the FCI or not.

It is worth noticing that the EU-DCLL design includes other MHD issues. They are mainly related with the 3D geometrical configurations, the electrical coupling between PbLi channels and with the fringing effect of the magnetic field. These effects must be studied in detail for computing the contribution of each issue to the whole MHD pressure drop. In particular, there are some geometries of the design that are not present in other DCLL concepts. As a consequence, they have not been studied in the past. These unique problems should be addressed in future with dedicated MHD analyses as the lack of experience makes difficult to estimate beforehand their importance.

8. Conclusions

MHD analyses for fully developed flows in rectangular section channels under EU-DCLL conditions have been performed. 3 different alumina-based FCI designs have been compared. Using the MHD velocity profile as an input, 3D heat transfer computations have been performed assuming convection boundary conditions for the helium channels.

Results show that the good electrical insulation properties of alumina are enough for electrically decoupling the bulk flow from gap flow. In other words, almost no currents cross through the FCI for the 3 designs. The thin sandwich FCI accomplishes this purpose effectively regardless the really thin alumina layer (0.1 mm). Sandwich-like FCIs exhibit jets in the side gap which entails a better cooling of the FW compared with the naked FCI. The naked design presents the best pressure drop mitigation but it also implies the highest heat losses to the He circuit.

9. Acknowledgments

This work has been carried out within the framework of the EUROfusion Consortium and has received funding from the Euratom research and training programme 2014-2018 under grant agreement No 633053. The views and opinions expressed herein do not necessarily reflect those of the European Commission. This work has been partially funded by the MINECO Ministry under project ENE2013-43650-R. F.R. Urgorri acknowledges a pre-PhD contract of the Spanish MINECO.

References

[1] L. V. Boccaccini, G. Aiello, J. Aubert, C. Bachmann, T. Barrett, A. Del Nevo, D. Demange, L. Forest, F. Hernandez, P. Norajitra, G. Porempovic, D. Rapisarda, P. Sardain, M. Utili, and L. Vala. Objectives and status of EUROfusion DEMO blanket studies. *Fusion Eng. Des.*, 109-111, Part B:1199–1206, 2016.

[2] H. John, S. Malang, and H. Sebening. DEMO-relevant test blankets for NET/ITER. Technical report, Kernforschungszentrum Karlsruhe, 1991.

[3] D. Rapisarda, I. Fernández, I. Palermo, M. Gonzalez, C. Moreno, A. Ibarra, and E. Mas de les Valls. Conceptual design of EU-DEMO dual coolant lithium lead equatorial module. *IEEE Trans. Plasma Sci.*, 44(9):1603–1612, 2016.

[4] I. Fernandez-Berceruelo, M. Gonzalez, I. Palermo, F.R. Urgorri, and D. Rapisarda. Large-scale behavior of sandwich-like FCI components within the EU-DCLL operational conditions. *Fusion Eng. Des.*, 2018.

[5] P. Norajitra, W. W. Basuki, M. Gonzalez, D. Rapisarda, M. Rohde, and L. Spatafora. Development of sandwich flow channel inserts for an EU DEMO dual coolant blanket concept. *Fusion Sci. Technol.*, 68(3):501–506, 2015.

[6] S. Smolentsev, N. B. Morley, and M. Abdou. Magnetohydrodynamic and thermal issues of the SiCf/SiC flow channel insert. *Fusion Sci. Technol.*, 50(1):107–119, 2006.

[7] I. Fernandez-Berceruelo, I. Palermo, F.R. Urgorri, L. Maqueda, D. Alonso, and J. Olalde. DCLL design report 2016. Technical Report EFDA-D-2MMM6Q, EUROfusion, 2017.

[8] S. Maland and K. Schleisiek. Dual coolant blanket concept. Technical Report KfK 5424, Kernforschungszentrum Karlsruhe, 1994.

[9] D. Rapisarda, I. Fernandez, I. Palermo, F.R. Urgorri, L. Maqueda, D. Alonso, T. Melichar, O. Frbort, L. Vla, M. Gonzalez, P. Norajitra, H. Neuberger, and A. Ibarra. Status of the engineering activities carried out on the european DCLL. *Fusion Eng. Des.*, 2017.

[10] S. Smolentsev, N. Morley, and M. Abdou. Code development for analysis of MHD pressure drop reduction in a liquid metal blanket using insulation technique based on a fully developed flow model. *Fusion Eng. Des.*, 73(1):83 – 93, 2005.

[11] I. Palermo, D. Rapisarda, I. Fernandez-Berceruelo, and A. Ibarra. Optimization process for the design of the DCLL blanket for the european DEMOnstration fusion reactor according to its nuclear performances. *Nucl. Fusion*, 57(7):076011, 2017.

[12] C. Mistrangelo and L. Bühler. Influence of helium cooling channels on magnetohydrodynamic flows in the HCLL blanket. *Fusion Eng. Des.*, 84:1323–1328, 2009.

[13] E. Mas de les Valls, L.A. Sedano, L. Batet, I. Ricapito, A. Aiello, O. Gastaldi, and F. Gabriel. Leadlithium eutectic material database for nuclear fusion technology. *J. Nucl. Mater.*, 376(3):353 – 357, 2008. Heavy Liquid Metal Cooled Reactors and Related Technologies.

[14] F. Gillemot, E. Gaganidze, and I. Szenthe. Material property handbook pilot project on EUROFER97(MTA EK, KIT). Technical Report EFDA-D-2MRP77, EUROfusion, 2016.

[15] B. Schulz. Thermophysical properties of the Li(17)Pb(83) alloy. *Fusion Engineering and Design*, 14(3):199 – 205, 1991.

[16] F. Tavassoli. Fusion demo interim structural design criteria appendiz a material design limit data A3.S18E eurofer steel. Technical report, DMN, 2004.

[17] P. Satyamurthy, P.K. Swain, V. Tiwari, I.R. Kirillov, D.M. Obukhov, and D.A. Pertsev. Experiments and numerical MHD analysis of LLCB TBM test-section with NaK at 1T magnetic field. *Fusion Eng. Des.*, 91(Supplement C):44 – 51, 2015.

[18] J. A. Shercliff. Steady motion of conducting fluids in pipes under transverse magnetic fields. *Math. Proc. Cambridge Philos. Soc.*, 49(1):136144, 1953.

[19] J. C. R. Hunt. Magnetohydrodynamic flow in rectangular ducts. *Journal of Fluid Mechanics*, 21(4):577–590, 1965.

[20] M. Ni, R. Munipalli, P. Huang, N. B. Morley, and M. Abdou. A current density conservative scheme for incompressible MHD flows at low magnetic reynolds number. part ii. *J. Comput. Phys.*, 2007.

[21] J. S. Walker. Magnetohydrodynamic flows in rectangular ducts with thin conducting walls. *Journal de Mécanique*, 20(1), 1981.

[22] H. C. Ji and R. A. Gardner. Numerical analysis of turbulent pipe flow in a transverse magnetic field. *Int. J. Heat Mass Transfer*, 40(8):1839–1851, 1997.

[23] V. Gnielinski. New equations for heat and mass transfer in turbulent pipe and channel flow. *Int. Chem. Eng*, 16(2):359–368, 1976.

[24] S. Smolentsev, R. Moreau, and M. Abdou. Characterization of key magnetohydrodynamic phenomena in PbLi flows for the US DCLL blanket. *Fusion Engineering and Design*, 83(5):771 – 783, 2008.

[25] J. Sannier, T. Flament, and A. Terlain. Corrosion of martensitic steels in flowing Pb17Li. *Fusion Technol.*, 3(7), 1990. Proceedings of the 16th Symposium on Fusion Technology.

[26] J. Konys, W. Krauss, H. Steiner, J. Novotny, and A. Skrypnik. Flow rate dependent corrosion behavior of Eurofer steel in Pb15.7Li. *J. Nucl. Mater.*, 417(1):1191 – 1194, 2011. Proceedings of ICFRM-14.

[27] S. Malang and M. S. Tillack. Development of self-cooled liquid metal breeder blankets. Technical Report FZKA 5581, Forschugszentrum Karlsruhe, 1995.